
THE CLASSIFICATION OF ALZHEIMER'S DISEASE AND MILD COGNITIVE IMPAIRMENT IMPROVED BY DYNAMIC FUNCTIONAL NETWORK ANALYSIS

A PREPRINT

Nicolas Rubido[§]

Aberdeen Biomedical Imaging Centre
University of Aberdeen

Venia Batziou[§]

Health Data Science
Swansea University Medical School
Swansea University

Marwan Fuad

Health Data Science
Swansea University Medical School
Swansea University

 **Vesna Vuksanović**^{*}

Health Data Science
Swansea University Medical School
Swansea University

Correspondence:vesna.vuksanovic@swansea.ac.uk

May 27, 2025

ABSTRACT

Brain network analysis using functional MRI has advanced our understanding of cortical activity and its changes in neurodegenerative disorders that cause dementia. Recently, research in brain connectivity has focused on dynamic (time-varying) brain networks that capture both spatial and temporal information on cortical, regional co-activity patterns. However, this approach has been largely unexplored within the Alzheimer's spectrum. We analysed age- and sex-matched static and dynamic fMRI brain networks from 315 individuals with Alzheimer's Disease (AD), Mild Cognitive Impairment (MCI), and cognitively-normal Healthy Elderly (HE), using data from the ADNI-3 protocol. We examined both similarities and differences between these groups, employing the Juelich brain atlas for network nodes, sliding-window correlations for time-varying network links, and non-parametric statistics to assess between-group differences at the link or the node centrality level. While the HE and MCI groups show similar static and dynamic networks at the link level, significant differences emerge compared to AD participants. We found stable (stationary) differences in patterns of functional connections between the white matter regions and the parietal lobe's, and somatosensory cortices, while metastable (temporal) networks' differences were consistently found between the amygdala and hippocampal formation. In addition, our node centrality analysis showed that the white matter connectivity patterns are local in nature. Our results highlight shared and unique functional connectivity patterns in both stationary and dynamic functional networks, emphasising the need to include dynamic information in brain network analysis in studies of Alzheimer's spectrum.

Keywords Dynamic Functional Connectivity · Alzheimer's Disease · Mild Cognitive Impairment · Random Forest Classifier · Brain Networks

Introduction

Brain networks derived from functional magnetic resonance imaging (fMRI) have improved our understanding of cortical functional connectivity, i.e., patterns of co-activity between remote cortical processes (Sporns, 2010; Fornito

* correspondence: vesna.vuksanovic@swansea.ac.uk Web: Vesna Vuksanovic

[§] These authors contributed equally

et al., 2016; Bijsterbosch and Beckmann, 2017). Mapping functional networks from neuroimaging data, has been useful in providing information about altered cortical activity in brain disorders (Mattson, 2000; Zecca et al., 2004; Pievani et al., 2011; Stam, 2014). In Alzheimer's disease (AD), functional networks differ from the patterns of connectivity observed in healthy individuals (Eguiluz et al., 2005; Damoiseaux et al., 2006; Honey et al., 2009; Bullmore and Sporns, 2009, 2012), and the magnitude of these differences often correlates with the underlying abnormal accumulation of missfolded tau protein and deposits of beta-amyloid, or white matter damage (Borne et al., 2024). Differences also correlate with the severity of clinical symptoms, assessed using cognitive and behavioral metrics (Stam et al., 2007; Binnewijzend et al., 2014; Luo et al., 2017; Dai et al., 2019; Lei et al., 2019). Network-based studies further demonstrate that while brain disorders like AD exert a global effect on the brain, their impact is heterogeneous, with certain regions, particularly the central (hub) areas of the temporal, parietal, and frontal regions associated with higher-order cognitive functions, being more severely affected (He et al., 2008; Stam et al., 2009).

Alzheimer's disease is increasingly recognised as a disconnection syndrome, disrupting brain networks and leading to cognitive and behavioral decline (Delbeuck et al., 2003). Network changes are observed in Mild Cognitive Impairment (MCI) (Zhang et al., 2011; Gilligan et al., 2019), a cognitive disorder that may progress to AD. However, the impact of MCI and AD is not always proportional to their cognitive severity. Both, MCI and AD, impact local (de Haan et al., 2012; Heringa et al., 2014) and small-world network metrics (Tijms et al., 2013; Seo et al., 2013) through changes in clustering (i.e., segregation) (Brier et al., 2014) and global efficiency (i.e., integration) (Lo et al., 2010; Yao et al., 2010; Reijmer et al., 2013). Betweenness centrality (Liu et al., 2012; Wang et al., 2020), modular organization (Chen et al., 2013; Contreras et al., 2019; Vuksanović et al., 2019; Vuksanović et al., 2019) and reduced functional connectivity within the default mode network (Greicius et al., 2004; Petrella et al., 2011; Agosta et al., 2012; Dillen et al., 2017), have also been consistent findings throughout studies.

Recently, dynamic brain network analysis, which considers temporal fluctuations in the resting-state fMRI signal, has revealed patterns of activity that are usually averaged out by conventional functional network analysis. These patterns of activity, termed dynamic functional networks (dFNs), reveal transient (metastable) dynamical states, whose flexible links (reconfiguration) support cognitive processing (Vuksanović and Hövel, 2014; Alderson et al., 2020). Analysis of dynamic functional networks from functional brain recordings, i.e., those acquired over a period of time, has shown the potential to reveal clinically relevant information (Filippi et al., 2019; Moguilner et al., 2021). For example, (He et al., 2018) demonstrated low flexibility of the language network in patients with temporal lobe epilepsy due to reduced metastability, which contributes to decreased verbal fluency. These findings highlight the importance of integrating temporal information into brain network analysis. However, in addition to a few recent studies (Rubido et al., 2024; Córdoba-Palomera et al., 2017; Quevenco et al., 2017; Núñez et al., 2021; Sendi et al., 2021), this approach remains largely unexplored in the context of functional network disruptions in the Alzheimer's spectrum. In addition, comparative analyses of static and dynamic FN in AD are lacking.

In this study, our aim was to investigate the potential of fMRI-derived cortical functional networks to assess disrupted connectivity in AD. Using comparative analysis of dynamic and static functional networks, we studied whether the temporal characteristics of functional connectivity are more effective than static ones in identifying reliable functional networks' features in individuals with AD compared to normal ageing and MCI. In addition, we examined sensitivity and specificity of these features to identify AD and MCI individuals from healthy elderly. We hypothesised that dFNs in AD behave differently compared to HC and MCI, reflecting disrupted functional connectivity patterns associated with AD.

Results

Static and Dynamic Functional Networks: the Link Level Analysis

Figure 1 shows statistically significant ($p \leq 0.05$) links across static functional networks (sFNs) based on the K-W test, where the links correspond realization-averaged p-values obtained from 100 K-W tests. Each test was performed on 50 randomly sampled single-subject correlations in each cohort (realizations) for the (i, j) -the node pair. There were 183 significant p-values that survived the tests, revealing differences at the link level for sFNs between the groups, which predominately map the functional connections between white matter (WM) and the parietal, frontal, and temporal lobes' regions. The parietal lobe shows significant differences in the static correlations of the Inferior and Superior parietal Lobules (IPL and SPL) and Primary and Secondary Somatosensory Cortices (PSC and SSC/Operculum parietal), where the most prevalent and significant differences appear in the connections between the SSC/OP to WM regions. The links connecting the frontal lobe and WM regions, show the differences predominantly in the primary motor cortex (PMC), whereas the links from the temporal lobe to WM regions show differences predominantly mainly in the primary auditory cortex (PAC) and the hippocampus formation (HPC).

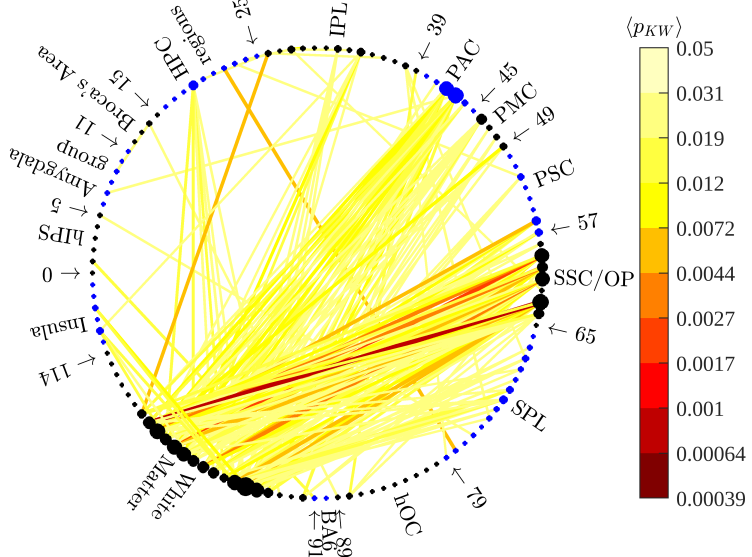


Figure 1: Static functional networks' differences at the link level within the three study groups. Links (i.e., pairwise correlations) were drawn between nodes of the Juelich Brain Atlas on the circle if they passed the Kruskal-Wallis tests applied to the each link's bootstrapped distributions. p-values are colour coded.

Figure 1 also represents a reference for inter-cohort analysis of static and dynamic functional networks (dFN), and the post-hoc, pairwise comparisons between the HC, MCI, and AD cohorts. In addition, using the K-W tests on the realisation-averaged p-values for dFNs (as shown in Fig. 2), can help to determine which dynamic correlation exhibit stationary characteristics and which demonstrate transient meta-stability across the cohorts. Specifically, significant p-values identified in the K-W tests for dFNs are considered static if they also appear in the K-W test for sFNs; otherwise, they are classified as transient, revealed through the sliding window analysis.

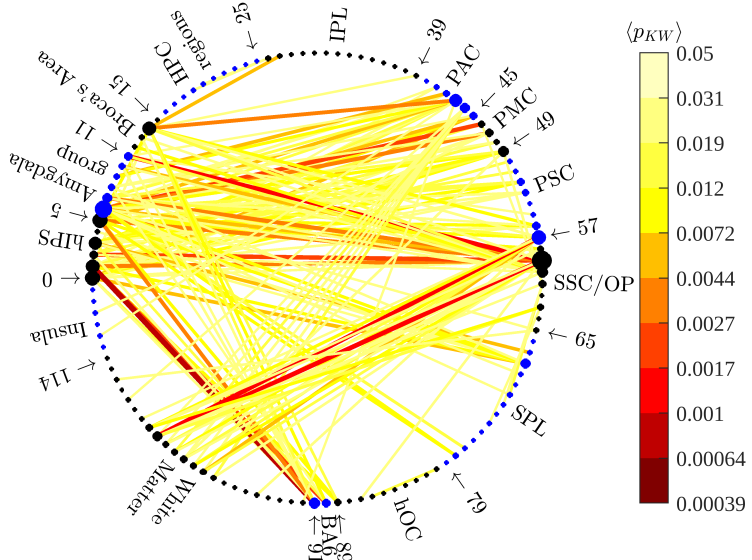


Figure 2: Dynamic functional networks' differences at the link level within the three study groups. Links (i.e., pair-wise correlations) were drawn between nodes of the Juelich Brain Atlas on the circle if they passed the Kruskal-Wallis tests applied to the each link's bootstrapped distributions. Dynamic functional connectivity was estimated using sliding windows of 60s in length. p-values are colour-coded.

Statistically different dynamic functional links are shown in Fig. 2. There were 148 links whose p-values $\langle p_{KW}(i, j; t_0 = 90, \Delta t = 20) \rangle \leq 0.05$ survived the K-W test of differences within the study group. The links

highlights patterns similar to those in Fig. 1. Although the strength in the connections from the WM regions to SSC/OP and PAC appears different from that in Fig. 1, the appearance of the links in Fig. 1 implies a stationary nature of these connections. Functional connections mapped using dFN analysis that are missing in Fig. 1, were found between Broca's Area, the Amygdala group, and the anterior Intra-parietal Sulcus (hIPs) with the SSC/OP, PSC, PMC, PAC, and Premotor Cortex (BA6), revealing temporal (meta-stable) nature of these connectivity patterns.

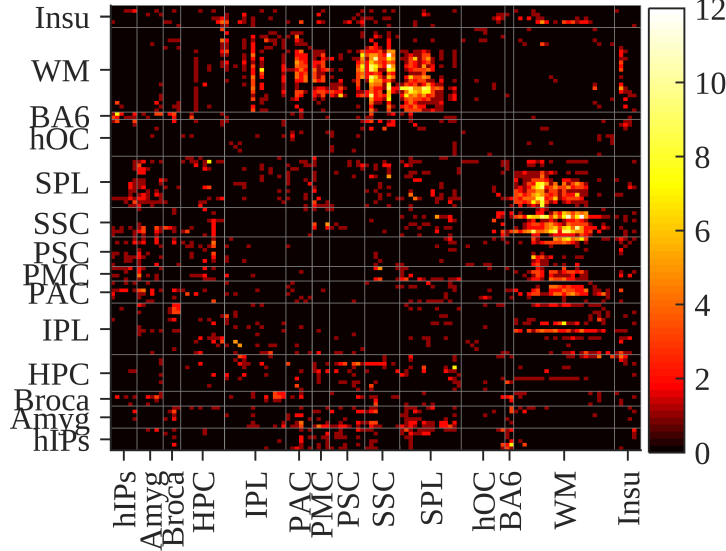


Figure 3: **Number of significant realisation-averaged p-values in the sliding-window analysis.** Number of times each realisation-averaged p-value is significant in all (18) sliding windows for each pair of the Juleich brain atlas regions.

In addition to dFNs analysis of differences within the study groups, we also show the frequency of significantly different tests (links) across sliding windows (i.e., how many times the distribution of correlations between a (i, j) cortical pair was statistically different as the window used for dFN analysis slides along the fMRI time series). The frequency ranges from 12 to 4 appearances, out of the maximum of 18 sliding windows.

Pair-wise analysis of the static networks between groups: the link level

A post-hoc analysis was performed on sFNs links on paired groups: AD/HC, AD/MCI and MCI/HC, using the ($p < 0.01$) significance level as for the K-W tests. There were 279 significantly different links for AD/HC [Fig. 4 (left)] and 150 significantly different links for MCI/HC [Fig. 4 (right)]. For the AD/MCI comparisons, there were 150 links that survived significance tests at the (<0.05) level and there were no significant links for the increased $p < 0.01$ level.

Fig. 4 (left panel) shows statistically different functional connections involve the White Matter (WM) regions, which connect to multiple gray matter (GM) regions, predominantly in the parietal, temporal and frontal lobes. The GM regions are: the Primary Auditory Cortex (PAC), Primary Motor Cortex (PMC), Primary Somato-sensory Cortex (PSC), Secondary Somato-sensory Cortex (SSC), and Superior parietal Lobule (SPL) regions. On the other hand, Fig. 4 (right panel) shows that the MCI/HC differences map out predominantly patterns of connections within GM. The connections include: the hippocampus formation (HPC) and the pre-motor cortex (BA6), the SPL with the Insula, and the PSC with the Inferior parietal Lobule (IPC) and HPC. Significantly different AD/MCI links (at $p < 0.05$) are between WM and GM regions – the SSC regions and Insula.

To establish confidence interval for these pair-wise tests on the between-groups differences, we repeated the tests on the resampled (bootstrapped) cohorts. We generated 100 bootstraps from each group by selecting ($N = 50$) participants (i.e., 50 from each group, matched by the corresponding male/female ratio between the groups). The results of this, more stringent statistical analysis, showed similar results: Most of the 248 links for HC/AD survived, and were found between the same WM and GM regions that also appear in Fig. 4 (left panel). Similarly, the 158 survived links for the AC/MCI comparisons were found between GM region highlighted in Fig. 4 (left panel). However, there were only 7 significantly different links for HC/MCI, and none of the tests survived multiple comparisons corrections of the p-values, which indicates that a larger cohort potentially corroborate these results.

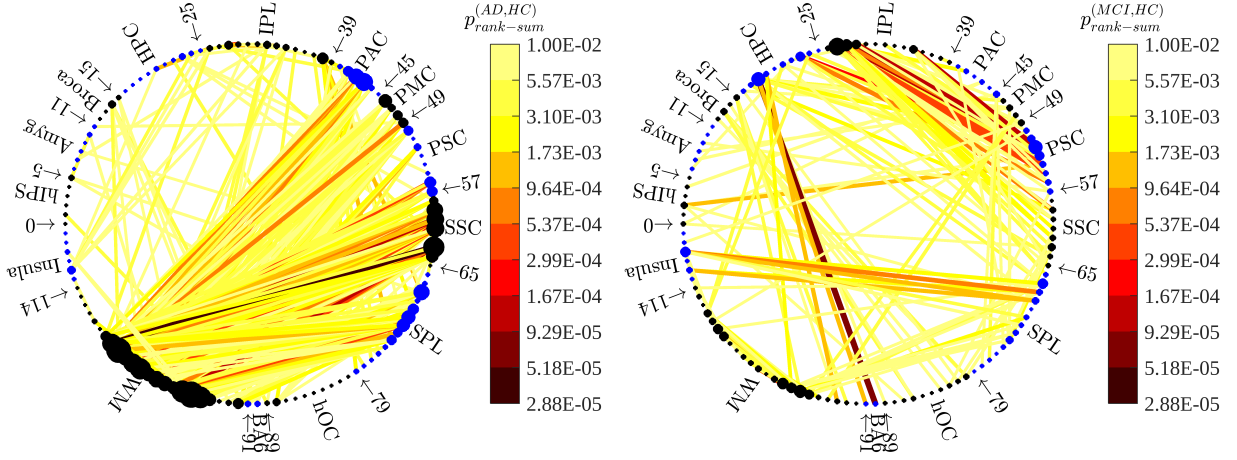


Figure 4: Significant differences at the link level between-groups: Alzheimer's disease (AD), mild cognitive impairment (MCI) and healthy controls (HC). Links (i.e., pair-wise correlations) were drawn between nodes of the Juelich Brain Atlas on the circle if they passed the Kruskal-Wallis tests applied to the each link's bootstrapped distributions (100 values for each test). p-values are colour-coded.

The static networks of the resampled groups at the link level: deviation from healthy controls

To investigate the deviation of functional correlations patterns in sFNs from healthy controls, (i.e., whether there is an increase or decrease in these correlations from HC), we visualised patterns of these changes in respect to the median sFN of the HC group. In Fig. 5 each cohort's median correlation for a pair of nodes were colour coded to illustrate the strength of the correlations. For example, the median value of the links between the SSC and WM regions for HC cohort is $\simeq 0$, meaning nearly uncorrelated functional activity between these regions. However, these became positive in AD, where we observed correlation values $\simeq 0.25$. Similarly, links between the PMC and WM have negative median values in HC $\simeq -0.25$, but became uncorrelated (i.e., $\simeq 0$) in AD. Simmilar patterns of these deviations from HC, can be in MCI [Fig. 5 (right panel)], however, the magintide of these deviations is smaller. Please see also Section Pair-wise analysis of the static networks between groups: the link level, where we show that there are 150 significant p-values between MCI and HC cohorts, but nearly as twice (279) between AD and HC cohorts.

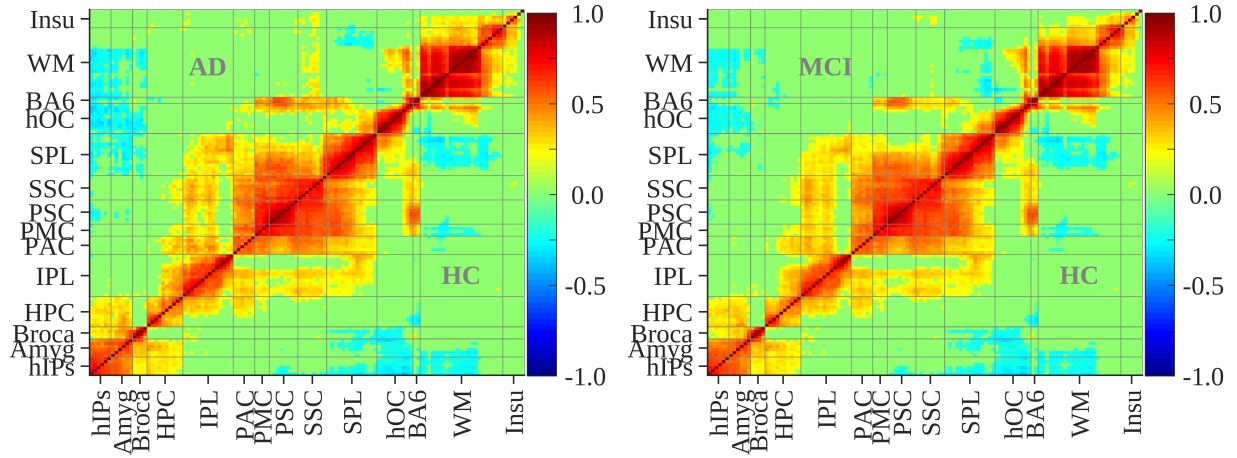


Figure 5: **Cohorts' median static correlations.** Upper diagonal entries show the median static correlation values (colour coded) for the AD/MCI cohort, and lower diagonal entries the same values for the HC cohort.

When comparing the sFNs between AD and MCI cohorts (data not shown), we saw similar pattern: higher correlations in ADs than in MCIs and 195 significant p-values for pair-wise correlations. Some interesting observations are: the WM and the SSC sFNs are close to zero for the MCI cohort – the same as for the HC cohort in the lower diagonal

entries of Fig. 5. In addition, the links between the WM regions and the Insula were significantly different only between AD ($r \simeq 0.50$) and MCI ($r \simeq 0.25$) cohorts, but there were no differences between HC and AD.

Inter-cohorts differences in dynamic functional networks: the link level

Fig. 6 shows dFN links' frequency count for between-cohorts differences, by summarising a significant inter-cohorts difference across the sliding windows (similar to Fig. 3 for within-cohort differences), where Fig. 6 (left) is for AD/HC and Fig. 6 (right) for MCI/HC.

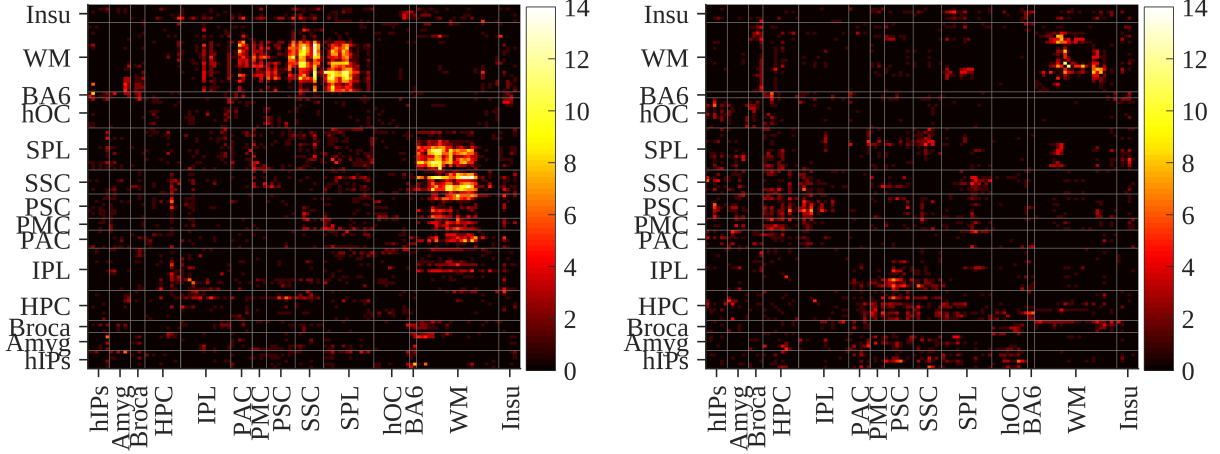


Figure 6: Inter-cohorts differences between static and dynamic functional networks (s/dFN) at the link level. Colour code represents the number of times a dFN link differ from a sFN link between AD/HC (left panel) and MCI/HC (right panel).

Consistent with our analysis, most of the inter-cohorts differences are driven by the connections of the WM with the SSC and the SSL regions for AD/HC, where there is the maximum of 14 appearances [found between the intra-hemispheric connection between nodes 63 (right secondary somatosensory cortex) and 107 (right optic radiation)] for AD/HC. High frequency was also found between WM and SPL regions, and between WM and PSC, PMC, and PAC regions. The right panel of Fig. 6 shows that the dFNs links' frequency between MCI and HC participants is high within the WM regions, where the inter-hemispheric connection between regions 100 and 101 (inferior occipito-frontal fascicle l/r) was different across 12 sliding windows.

For AD/MCI differences (data not shown), we found that the functional connection between nodes 63 and 107 was significant across 12 sliding windows, which is the result the same as for AD/HC. However, some GM to GM connections were different from those in AD/HC. For example, differences in the links between the IPL with Broca's Area and the PAC with Amygdala, which were not found in MCI/HC or AD/HC.

Fig. 6 (left panel) shows that the frequency of significant links in dFNs for AD/HC follows the pattern similar to the sFNs analysis [see Fig. 3]. However, this is not the case for MCI/HC, where the dFNs analysis [see Fig. 6 (right panel)] highlights changes within the WM networks, whilst the sFNs analysis, [see Fig. 4], highlights connections within the GM networks.

The dynamic networks on the resampled groups at the link level: changes from healthy controls

Similarly to the analysis for sFNs (showed in Fig. 5), we visualised deviation of dFNs links with respect to the HC group. In terms of the direction of the deviation, the results were less consistent than in sFNs, than those for the sFNs. That is, some of the correlations increase and other decrease (see Fig. 7), which indicates that non-stationary variations in the functional connections are missed in static analysis.

For example, we saw that the functional connections between the SPL and WM regions for the HC cohort that have negative median correlation values $\simeq -0.25$ (top panels in Fig. 7), while these connections were still present in MCI cohort they disappear in AD $\simeq 0$ (see top left panel of Fig. 7). Similarly, the IPL and SSC regions regions were not connected with the WM regions in HC or MCI ($\simeq 0$), but in AD the connections between them were positive $\simeq 0.25$, which is similar behaviour to that observed for the sFNs. However, differences appear between IPL and SPL connections in the first window [Fig. 7 (upper panels)] in HC and AD, while this deviation was not observed in MCI.

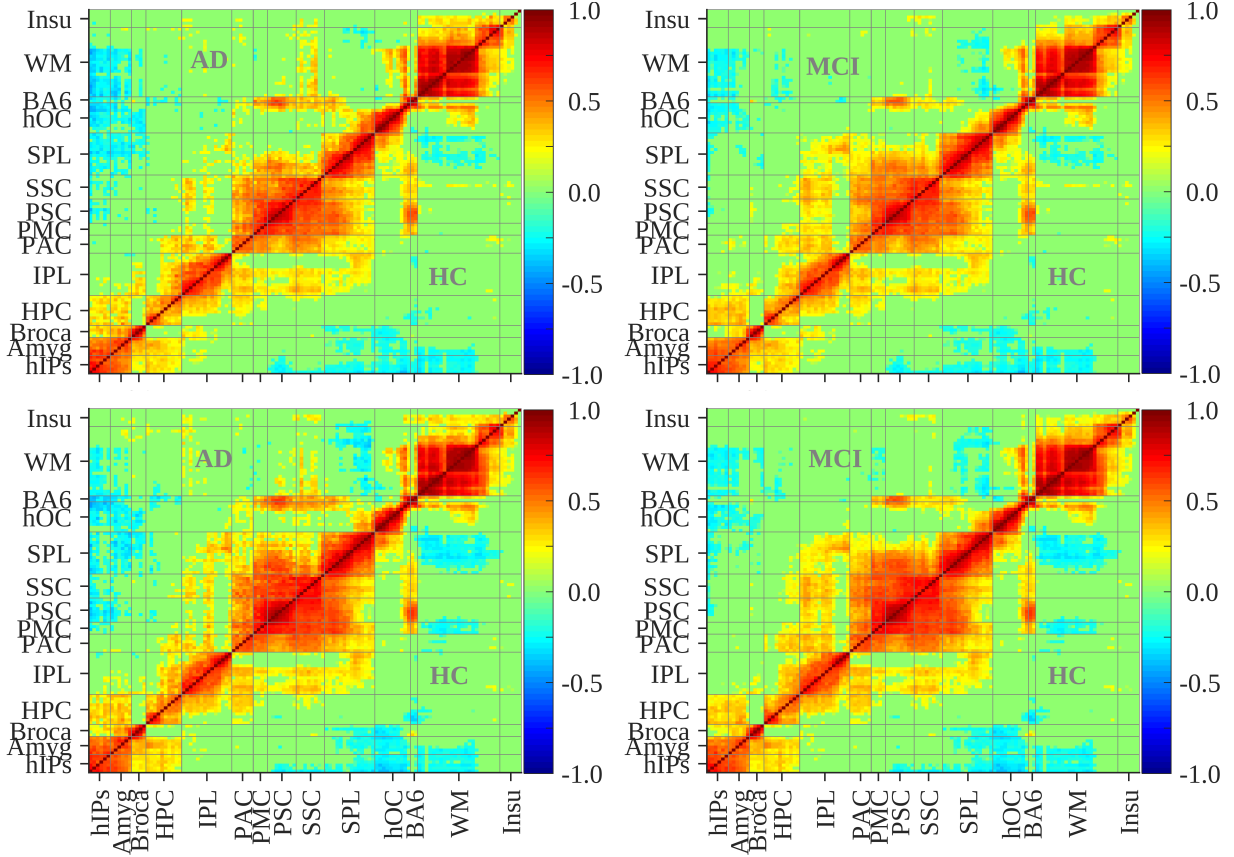


Figure 7: **Cohorts' median sliding-window correlations.** Left panels: median values for AD (upper diagonal elements) and HC (lower diagonal elements) cohorts of the correlations. Right panels: median values for MCI (upper diagonal elements) and HC (lower diagonal elements) cohorts. Only data for first (top) and last (bottom) sliding windows are shown.

Similarly, the PSC and SSC regions were not connected to the WM region in HC and MCI [Fig. 7 (lower panels)], but they were positively correlated in AD. Another notable non-stationary deviation is in the PSC and the Amygdala group links, which were $\simeq 0$ in HC and MCI, but negative in AD $\simeq -0.3$.

Dynamic and Static Functional Networks: Node Degree and Eigenvector Centrality Metrics

Fig. 8 shows analysis of two measures of network centrality – node degree and eigenvector centrality – between sFN (top panels) and dFNs (bottom panels) within the three groups. Visually, there are only a few differences between sFN and dFN centrality measures. Most of the significant differences in node degree, for both sFN and dFN, were found between the WM regions (grey bands and asterisk in the plots), where some differences overlap between the two networks (s/d). We interpret the non-overlapping dFN nodes that become stationary in sFNs as those with the metastable dynamic. These nodes are the HCP, IPL and Insula.

Eigenvector centrality shows similar behaviour of both, the sFNs and dFNs [Fig. 8 (right panels)] however, only the sFN reached significant differences for four nodes (Amygdala, HPC, SPL and hOC). The most striking result is lack of significant differences within the WM regions, which was almost a constant in all other analysis. We interpret this that all differences in the WM regions are local in nature and that they disappear when looking at the centrality measure which takes into account global connectivity.

Random Forest Classification

Table 1 shows the results of the RF models trained on BOLD time series data. We classified the time series using three different classes of inputs: (i) set of nodes from 7 to 26, i.e., nodes of the amygdala and hippocampal

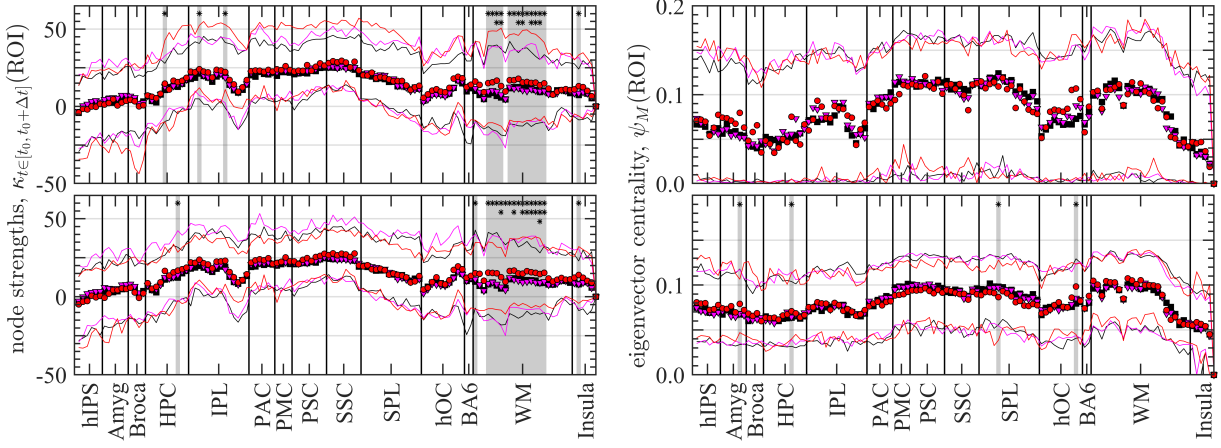


Figure 8: **Weighted node centrality measures for static and dynamic functional brain networks.** Left panels: node strength of the Jülich Brain Atlas, where vertical lines reference the ROI endings and shaded areas highlight significantly different medians between HC and AD cohorts (*: $0.001 < p \leq 0.01$, **: $10^{-4} < p \leq 0.001$, and ***: $p \leq 10^{-4}$). Top [Bottom] panels: centrality values for the static [dynamic] correlations that use all the BOLD signal [use sliding windows with $t_0 = m \Delta t/2$, $\Delta t = 20$, and $m = 0, 1, \dots, 17$]. The centrality values for the dFN of each participant (bottom panels) are here averaged over the 18 sliding windows. Filled symbols represent the cohort's median value for each ROI and continuous lines the interval containing 95% of the cohort's centrality values. The median values for HC are shown by black squares, for MCI by purple triangles, and for AD by red circles, with their respective 95% lines in the same colours.

formation, which were found to be relevant for metastable (temporal) networks, (ii) set of WM nodes (92 to 114), significantly different in terms of stable (stationary) patterns, and (iii) a subset of nodes in WM – nodes 95 to 112 – that were found to be different. The classifier was used on the whole time series of 197 points and windows of $\Delta t = 20$, 40 and 60s. In general, the RF classifiers preformed better when only two groups were pooled together, achieving the highest accuracy of $\approx 76\%$ between HC and AD groups for the first set of nodes (of the amygdala and hippocampus formation) and also for the third set of nodes (WM nodes 95 to 112) for $\Delta t = 60$ s. Across all configurations, the highest accuracies were consistently achieved with a window size of $\Delta t = 60$ s, including an accuracy of approximately 74% – the best result for three-group classification – and a significant improvement over previous results (Son et al., 2017).

Nodes	Groups	Accuracy (%)			
		T= 197	$\Delta t = 20$	$\Delta t = 40$	$\Delta t = 60$
7 – 26	MCI vs AD	50.6 \pm 3.1	52.8 \pm 1.7	53.0 \pm 4.1	58.8 \pm 3.1
	MCI vs AD	73.6 \pm .8	73.6 \pm .8	73.1 \pm 1.2	73.6 \pm 1.1
	HC vs AD	75.5 \pm .7	75.4 \pm .7	75.4 \pm .7	79.4 \pm 1.4
	HC + MCI + AD	46.4 \pm 2.2	45.4 \pm 3.2	44.8 \pm 3.0	57.8 \pm 2.5
92 – 114	MCI vs AD	73.6 \pm .8	73.6 \pm .8	73.6 \pm .8	74.2 \pm 1.1
	MCI vs HC	52.6 \pm .3	53.1 \pm 1.7	53.2 \pm 2.1	71.8 \pm 2.0
	HC vs AD	75.4 \pm .7	75.4 \pm .7	75.4 \pm .7	78.7 \pm 1.2
	HC + MCI + AD	45.8 \pm 2.6	47.6 \pm 2.1	50.0 \pm 1.5	63.0 \pm 2.5
95, 96, 100:108,111, 112	HC vs AD	75.5 \pm 0.8	75.5 \pm 0.8	75.5 \pm 0.8	76.5 \pm 1.1
	HC vs MCI	55.5 \pm 2.1	49.1 \pm 2.1	53.2 \pm 2.4	68.5 \pm 2
	AD vs MCI	45.4 \pm 3	50.2 \pm 3.1	42.5 \pm 2.5	67.5 \pm 2
	HC vs (AD + MCI)	54.0 \pm 2.0	47.6 \pm 2.0	52.7 \pm 2.6	74.3 \pm 3.2

Table 1: The accuracy of the Random Forest classifier on the entire time series of 197 time points and on windows of $\Delta t = 20$, 40 and 60 points, reported as the mean \pm standard error. The classifier was trained using 10-Fold Cross-Validation based on 100 decisions trees. For the nodes names see the SI Table 1.

Discussion

In this study, we conducted static and dynamic analyses of cortical functional networks, derived from fMRI data, in a cohort of 315 individuals from three, age- and sex-matched, clinical groups: Alzheimer's disease, mild cognitive impairment, and healthy older adults. Our analyses suggest that combining information from static and dynamic functional networks offers a more complete picture of brain connectivity and its changes in people with dementia and cognitive impairment.

Our comparative analysis of sFNs and dFNs highlighted distinct drivers of local and global functional connectivity patterns between groups. For example, while white matter regions displayed consistent connectivity differences across groups, these differences were not evident in nodal centrality measures that drive global (network) connectivity. In addition, static functional networks revealed significant differences in connectivity at the link level across the three groups, particularly in connections between white matter and the somatosensory, primary auditory, and hippocampal cortices. This contrasts dynamic functional networks (dFNs), whose transient connectivity changes and meta-stable states, which are not detectable with static analysis, revealed differences in connectivity between the amygdala and inferior parietal and prefrontal cortex and hippocampal formation between AD and MCI individuals.

Studies have suggested that dFNs can reveal clinically relevant information by highlighting variations in connectivity that occur over shorter time scales (Rubido et al., 2024; Demirtaş et al., 2017). For example, dFNs have been a better predictor of cognitive impairment in AD, compared to conventional static FNs (see, e.g., (Du et al., 2018)), and have improved classification of AD from MCI or HC subjects (Quevenco et al., 2017; Du et al., 2018). It has been suggested that these improvements are based on the dFNs ability to better capture the flexibility and adaptability of functional networks to reconfigure on cognitive demands (Zhang et al., 2023; Gonzalez-Castillo and Bandettini, 2018). Some of our findings that are worth discussing in the context of dFN features as biomarkers of differences between AD and MCI are: (i) consistent inter-cohort differences driven by the connectivity patterns between the WM regions and somatosensory cortices, (ii) appearance of (temporal) links between the Broca area and amygdala with the hippocampal formation and (iii) strikingly similar results for network centrality metrics between sFN and dFN revealing that the WM functional connections are local in nature.

The most consistent results are the inter-cohort differences that are driven by the connectivity patterns between the WM regions and somatosensory cortices (Figs. 1,2,3,4 and 6). This is an interesting finding, as it is generally thought that AD spares primary sensory function. However, recent findings suggest that such interpretations have been drawn from a literature that has rarely taken into account variability in cognitive decline seen in AD patients (Wiesman et al., 2021). Cognitive domains affected by AD, are now known to modulate cortical somatosensory processing; that is, it is possible that abnormalities in somatosensory function in patients with AD have been suppressed by neuropsychological variability not accounted for in previous research. Supporting this hypothesis are recent studies that have revealed a dynamic interplay between somatosensory neural systems and the pre-frontal cortex that support attention and executive functions (Assem et al., 2024). Patients with AD often have impaired attention and executive functions, but these impairments are highly variable between individuals, and it is possible that controlling for variability in these cognitive abilities would reveal differences in somatosensory processing in these patients, as suggested by (Wiesman et al., 2021). Our findings suggest that dFN could be used as a biomarker of decline in AD, which is independent of their (subjective) cognitive scores.

Another interesting finding is the appearance of (temporal) links between the Broca area and the amygdala with the hippocampal formation (Fig. 2). The importance of the amygdala-hippocampal connections and its role in AD, has been well documented (for review, see (Song, 2023)). For example, impaired amygdala-hippocampus connectivity in AD is associated with impaired cognitive functions such as episodic and emotional memory, working memory formation, and anxiety and depression. It is also associated with patho-physiological abnormalities in tau protein hyperphosphorylation, impaired insulin signaling, $A\beta$ plaque formation, synaptic failure, and imbalanced cholinergic neuron innervation (Song, 2023). Again, dFN analysis was able to identify these 'hidden' patterns of activity in AD patients, which were concealed by longer, stationary brain processes.

Finally, our comparative analysis has revealed that the variability in eigenvector centrality, which has been identified as "an early biomarker of the interplay between early Alzheimer's disease pathology and cognitive decline" in healthy individuals (Lorenzini et al., 2023), is driven by temporal FNs identified through the link level analysis. Lorenzini et al., demonstrate that changes in EC, as well as EC variability over time, are involved in the neurofunctional manifestation of the early stages of Alzheimer's disease. Here, we provide evidence that EC differences were driven by the amygdala-hippocampus formation connectivity, which has been identified as an indicator of abnormal brain function in early AD (Laakso et al., 1995).

In this study, we used dFNs to investigate temporal fluctuations and transient (meta-stable) patterns of brain activity, in age- and sex-matched AD, MCI and healthy elderly individuals. In a comparative analysis study between sFN and

dFN, we provided evidence for similarity and differences between the two methods. We found consistent inter-cohort differences driven by the connectivity patterns between the WM regions and somatosensory cortices, indicating their stationary nature. dFNs revealed temporal characteristics of the links between the amygdala and the hippocampal formation, associated with neuropathological as well as cognitive hallmarks of AD. Explanation of the differences in variations of centrality metrics between sFN and dFN, revealed that the WM links are local in nature.

Methods

Participants and Cohorts

Data used in this study were obtained from the Alzheimer’s Disease Neuroimaging Initiative (ADNI) data base. We downloaded demographic, clinical and MRI data from $N = 315$ individuals participating in the study. The main inclusion criterion was that the fMRI datasets were acquired using the same resting-state protocols (see the Imaging Datasets Section for details). The 315 participants were selected from three groups: Healthy Controls (HC), Mild cognitive Impairment (MCI), and Alzheimer’s Disease (AD) groups. Demographic and clinical characteristics of the participant averaged across each group were shown in Table 2.

Demographics	HC	MCI	AD
Number of participants	141	128	46
Age (s.d.)	79.52 (5.60)	76.77 (4.72)*	78.46 (5.91)
Sex (F:M)	68 : 73	52 : 76	17 : 29
Clinical Scores			
MMSE (s.d.)	28.19 (3.64)	27.57 (2.47)	22.39 (3.84)*, **

Table 2: Participants’ demographic and clinical characteristics. Abbreviations: M-male, F-Female, s.d.-standard deviation, HC-healthy controls, AD-Alzheimer’s Disease, MCI-Mild Cognitive Impairment, * significant difference ($p < 0.01$) from HC. ** significant difference (i.e., $p < 0.01$) from MCI.

Imaging Datasets and Processing

We analysed resting-state functional (rs-fMRI) images from 315 participants. fMRI were acquired using ADNI-3’s basic EPI-BOLD protocol (details at ADNI’s website) and in (Weiner et al., 2017). In short, the scanning time of each participants was for up to 10 minutes using the same two-time accelerated 3 T scanner, following an even/odd interleaved axial-slicing (inferior to superior) of 3.4 mm with $(3.4375 \text{ mm})^2$ pixels ($\text{FOV} = 220 \times 220$; $P \gg A$ phase encoding; $\text{TE} = 30 \text{ ms}$; $\text{TR} = 3 \text{ s}$).

Image preprocessing, which includes brain extraction, registration in standard MNI space, and brain tissue segmentation was carried out using FMRIB’s pipeline *fsl_anat* in its default settings. Pre-processing of fMRI is done by applying FMRIB’s Expert Analysis Tool, *FEAT*, resulting in Blood-Oxygen-Level-Dependent (BOLD) signals of $N_T = 197$ data points ($197 \times \text{TR}$ acquisition times) for each voxel.

Networks Construction: Static and Dynamic Functional Connectivity

Cortical regions – defining the network nodes – are based on the Harvard-Oxford (H-OA) (?) and Jülich (JA) (Amunts et al., 2020) brain atlases, resulting in 2 independent cortical parcellations with $N_{ROI} = 48$ and 120 regions, respectively (details of the atlases in ??). The signal of each node is calculated by averaging the rs-fMRI BOLD time series across all voxels within the corresponding region/node.

Functional links were defined by the Pearson correlation coefficient, r (Sporns, 2010; Fornito et al., 2016; Pearson, 1895), calculated pairwise between all nodes,

$$r_{t \in [t_0, t_0 + \Delta t]}^{(s)}(i, j) = \text{cov} \left[x_{t \in [t_0, t_0 + \Delta t]}(i)^{(s)}, x_{t \in [t_0, t_0 + \Delta t]}(j)^{(s)} \right] / \sigma_i \sigma_j, \quad (1)$$

where $\text{cov} \left[x_{t \in [t_0, t_0 + \Delta t]}(i)^{(s)}, x_{t \in [t_0, t_0 + \Delta t]}(j)^{(s)} \right]$ is the covariance between the time window $[t_0, t_0 + \Delta t]$ of the node signals i and j (from t_0 to $t_0 + \Delta t$, where $t_0 + \Delta t \leq N_T = 197$), σ_i and σ_j are standard deviations of nodes i and j , and s is an index identifying participants from the cohorts. We also set a $p < 0.01$ significance threshold for the value $r_{t \in [t_0, t_0 + \Delta t]}^{(s)}(i, j)$ (see Eq. (1), which discards spurious correlations. This definition of functional links results in

a single subject, symmetric (undirected), weighted (with positive and negative weights), functional network, containing only statistically significant connections due to the removal of spurious correlations.

To construct links of static functional network, we utilise node signals in Eq. (1) (i.e., $[t_0, t_0 + \Delta t] = [0, N_T]$); that is all 197 points of the BOLD signal of a node (Sporns, 2010; Fornito et al., 2016; Lei et al., 2019; Gilligan et al., 2019; Seo et al., 2013; Brier et al., 2014). Because of the the $p < 0.05$ significance threshold, which was set in Eq. (1), approximately 35% and 39% were discarded from each participant's sFN for O-HA and JA, respectively.

To construct dynamic functional network (dFN), we use half-overlapping sliding windows of the node signals as described in (Leonardi and Van De Ville, 2015). This way, to maintain nominal control of mapping spurious (false positive) correlations within the time windows, the window size was determined by calculating 1/smallest frequency in the data, represented by the high-pass filter cutoff (Zalesky and Breakspear, 2015). Specifically, we set $t_0 = m \Delta t / 2$ in Eq. (1), with $m = 0, 1, \dots < N_T / \Delta t$ and $\Delta t = 20, 40$, or 60 data points – accounting for 1, 2, or 3 minutes of scan time, respectively. For a given window size Δt , the functional link $r_{t \in [t_0, t_0 + \Delta t]}^{(s)}(i, j)$ changes according to sliding-window time t_0 . The significance threshold for the (i, j) -th dynamic link for each participant was set based on the value obtained from its static counterpart: $r_{t \in [0, N_T]}^{(s)}(i, j)$. In this way the thresholds of the sliding-window correlations were set to be either greater or equal from the corresponding static correlations. As a result, for a sliding window of $\Delta t = 20$ points – resulting in 18 half-overlapping windows – used for the H-OA, the average percentage of discarded links per participant in its dFN is 28%. In comparison, when the same approach was used with the JA, the average percentage of discarded links was 30% (see Fig. 2).

Functional Networks' Metrics

We characterised functional connectivity in three study groups depending on the importance of the network nodes. A straightforward method to assess the importance of a network node is to compute its centrality. The centrality of a node is a measure that quantifies how important or influential a node is within a network. Centrality can be expressed in various ways; thus, there are multiple types of centrality measures. We characterised the importance of each node in the dFNs and sFN of each individual in the cohort by calculating the node strength and eigenvector centrality. Both centrality measures, node strength and eigenvector centrality, were calculated on the same number of links (network density) across all individual networks. This was done to preserve

Node Strength The simplest measure of network centrality is the so-called degree centrality, or simply node degree, which represents the number of connections a node has with other nodes in the network. In weighted networks – those of interest here – this becomes the node strength (or weighted degree), which measures the strength of the functional connections of node i . That is, the node strength $\kappa_{t \in [t_0, t_0 + \Delta t]}^{(s)}(i)$ (see Eq. 2) quantifies the strength of the functional connections (defined by Eq. 1) of the node i for the s -th participant in a cohort.

$$\kappa_{t \in [t_0, t_0 + \Delta t]}^{(s)}(i) = \sum_{j=1, j \neq i}^{N_{ROI}} r_{t \in [t_0, t_0 + \Delta t]}^{(s)}(i, j), \text{ with } i = 1, \dots, N_{ROI}. \quad (2)$$

Eigenvector Centrality Eigenvector centrality is the centrality measure based on the assumption that connections to more influential nodes are more important than connections to less relevant nodes, while also taking into account the centrality of their neighbours (). In simple terms, eigenvector centrality is the principal eigenvector of the network, which explains most of the variance in the data. Its principle is that links from important nodes (as measured by node strength) are worth more than links from unimportant nodes. All nodes start off equally, but as the computation progresses, nodes with more links gain importance. Their importance also influences the nodes to which they are connected to. After recomputing many times, the values stabilize and give the final eigenvector centrality values.

In general, an $M \times M$ non-singular, real-value matrix \mathbf{B} can be decomposed into M independent eigenvectors $\vec{\psi}_m$ with associated eigenvalues λ_m , such that $\mathbf{B} \vec{\psi}_m = \lambda_m \vec{\psi}_m$ with $m = 1, \dots, M$ (if the matrix is – as in our case – symmetric, then the eigenvalues are real-valued numbers). The eigenvector centrality network measure (Fornito et al., 2016) is given by the eigenvector associated with the largest eigenvalue ($\max_m \{\lambda_m\} = \lambda_M > 0$). The elements of this eigenvector provide a global measure of the relative importance of each node in the network, taking into account all connections in the network, not just those directly linked to node i . Using the single-subject correlation matrix $r_{t \in [t_0, t_0 + \Delta t]}^{(s)}$, the eigenvector centrality for the s -th participant was calculated as follows:

$$e_{t_\Delta}(i) = \frac{1}{\lambda_{t_\Delta}} \sum_{j=1}^{N_{node}} \rho_{t_\Delta}(i, j) e(j)_{t_\Delta}, \quad (3)$$

where λ_{t_Δ} is a constant that denotes the largest eigenvalue of ρ_{t_Δ} and $e_{t_\Delta}(i)$ denotes the i -th coordinate of the corresponding principal eigenvector; that is, a centrality score $e_{t_\Delta}(i)$ for each node i in an undirected network that fulfills $\varrho_{t_\Delta} \vec{e}_{t_\Delta} = \lambda_{t_\Delta} \vec{e}_{t_\Delta}$. Thus, the eigenvector centrality $e_{t_\Delta}(i)$ of a node i is given by the weighted sum of the values within the principal eigenvector of direct neighbours, $\rho_{t_\Delta}(i, j) e_{t_\Delta}(j)$, and scaled by the proportionality factor $\lambda_{t_\Delta}^{-1}$. Here, $\rho_{t_\Delta}(i, j)$ is an element of the correlation matrix representing the strength of the pair-wise interaction between nodes i and j during the sliding window $t_\Delta = t \in [t_m, t_m + \Delta t]$, defining a time-varying vector \vec{e}_{t_Δ} , whose elements are the $e_{t_\Delta}(i)$.

Statistical Analysis

Differences within FN and dFN across the cohorts We analysed differences at the individual-link level across cohorts using the non-parametric Kruskal-Wallis (KW) test (Kruskal and Wallis, 1952). To generate confidence interval for the test, we created 100 independent cohort realisations – each realisation randomly selects total of 150 participants from AD, MCI, and HC study groups, i.e., 50 from each ones. The selection was done in a way that a 15 : 35 female-to-male ratio was preserved in each sample of 50 participants. In more details, a single test was performed on 150 pair-wise correlations/network links $r_{t \in [t_0, t_0 + \Delta t]}^{(s)}(i, j)$, where $s = 1, \dots, 150$ from the three re-sampled cohorts. We conclude a difference in functional connectivity across cohorts if the averaged static or dynamic p-value is below 0.05.

Differences within sFN and dFN between the cohorts In the *ad-hoc* analysis we performed the test of pair-wise differences between the three groups using the the non-parametric Wilcoxon rank-sum (RS) test (Gibbons and Chakraborti, 2020). This was done for sFN and dFN separately. Similarly to the K-W test described above, the differences were tested on individual correlations/network links. We accepted differences for each test to be significant at the level $p < 0.01$.

Random Forest Classifier

A random forest classifier was employed to distinguish between individuals with AD, MCI and HC based on their fMRI time series. To train the classifier we used the entire time series of 197 time points, or windows of 20, 40 and 60 points, from 120 JBA regions. For the purpose of classification, a subset of these regions – selected based on prior relevance – was used as the feature of interest and input to the model. The classifier leveraged region-specific time series features to capture distinguishing patterns in functional activity associated with each group, enabling group differentiation. The selection of regions was decided by statistical analyses of dFC and sFC networks, with regions/nodes showing significant group differences included in the input for the RF model. After the selection of the nodes for analysis, we reshaped the time series in order to include every time point as a separate feature. We then added the labels based on AD, MCI or HC clinical groups and we trained a RF classifier using stratified 10-Fold Cross-Validation. The classifier averages the results of 100 decision trees.

Acknowledgments

N.R and M.F were supported by RSAT (Grant No. DSR1058-100), V.B. was funded by DSR1085-100.

Author Contribution

N.R. analysed the functional MRI data, prepared figures, and drafted the initial methods and results sections. V.B. performed the random forest (RF) analysis, with M.F. contributing the same RF analysis on the dataset. V.V. supervised the project, conceptualised the study, and wrote the final manuscript.

References

F. Agosta, M. Pievani, C. Geroldi, M. Copetti, G. B. Frisoni, and M. Filippi. Resting state fmri in alzheimer's disease: beyond the default mode network. *Neurobiology of aging*, 33(8):1564–1578, 2012.

T. H. Alderson, A. L. Bokde, J. S. Kelso, L. Maguire, and D. Coyle. Metastable neural dynamics underlies cognitive performance across multiple behavioural paradigms. *Human brain mapping*, 41(12):3212–3234, 2020.

K. Amunts, H. Mohlberg, S. Bludau, and K. Zilles. Julich-brain: A 3d probabilistic atlas of the human brain’s cytoarchitecture. *Science*, 369(6506):988–992, 2020.

M. Assem, S. Shashidhara, M. F. Glasser, and J. Duncan. Basis of executive functions in fine-grained architecture of cortical and subcortical human brain networks. *Cerebral Cortex*, 34(2):bhad537, 2024.

J. Bijsterbosch and C. Beckmann. *An introduction to resting state fMRI functional connectivity*. Oxford University Press, 2017.

M. A. Binnewijzend, S. M. Adriaanse, W. M. Van der Flier, C. E. Teunissen, J. C. De Munck, C. J. Stam, P. Scheltens, B. N. Van Berckel, F. Barkhof, and A. M. Wink. Brain network alterations in alzheimer’s disease measured by eigenvector centrality in fmri are related to cognition and csf biomarkers. *Human brain mapping*, 35(5):2383–2393, 2014.

L. Borne, R. Thienel, M. K. Lupton, C. Guo, P. Mosley, A. Behler, J. Giorgio, R. Adam, A. Ceslis, P. Bourgeat, et al. The interplay of age, gender and amyloid on brain and cognition in mid-life and older adults. *Scientific Reports*, 14(1):1–15, 2024.

M. R. Brier, J. B. Thomas, A. M. Fagan, J. Hassenstab, D. M. Holtzman, T. L. Benzinger, J. C. Morris, and B. M. Ances. Functional connectivity and graph theory in preclinical alzheimer’s disease. *Neurobiology of aging*, 35(4):757–768, 2014.

E. Bullmore and O. Sporns. Complex brain networks: graph theoretical analysis of structural and functional systems. *Nature reviews neuroscience*, 10(3):186–198, 2009.

E. Bullmore and O. Sporns. The economy of brain network organization. *Nature Reviews Neuroscience*, 13(5):336–349, 2012.

G. Chen, H.-Y. Zhang, C. Xie, G. Chen, Z.-J. Zhang, G.-J. Teng, and S.-J. Li. Modular reorganization of brain resting state networks and its independent validation in alzheimer’s disease patients. *Frontiers in human neuroscience*, 7:456, 2013.

J. A. Contreras, A. Avena-Koenigsberger, S. L. Risacher, J. D. West, E. Tallman, B. C. McDonald, M. R. Farlow, L. G. Apostolova, J. Goñi, M. Dzemidzic, et al. Resting state network modularity along the prodromal late onset alzheimer’s disease continuum. *NeuroImage: Clinical*, 22:101687, 2019.

A. Córdova-Palomera, T. Kaufmann, K. Persson, D. Alnæs, N. T. Doan, T. Moberget, M. J. Lund, M. L. Barca, A. Engvig, A. Brækhus, et al. Disrupted global metastability and static and dynamic brain connectivity across individuals in the alzheimer’s disease continuum. *Scientific reports*, 7(1):1–14, 2017.

Z. Dai, Q. Lin, T. Li, X. Wang, H. Yuan, X. Yu, Y. He, and H. Wang. Disrupted structural and functional brain networks in alzheimer’s disease. *Neurobiology of aging*, 75:71–82, 2019.

J. S. Damoiseaux, S. Rombouts, F. Barkhof, P. Scheltens, C. J. Stam, S. M. Smith, and C. F. Beckmann. Consistent resting-state networks across healthy subjects. *Proceedings of the national academy of sciences*, 103(37):13848–13853, 2006.

W. de Haan, W. M. van der Flier, H. Wang, P. F. Van Mieghem, P. Scheltens, and C. J. Stam. Disruption of functional brain networks in alzheimer’s disease: what can we learn from graph spectral analysis of resting-state magnetoencephalography? *Brain connectivity*, 2(2):45–55, 2012.

X. Delbeuck, M. Van der Linden, and F. Collette. Alzheimer’s disease as a disconnection syndrome? *Neuropsychology review*, 13(2):79–92, 2003.

M. Demirtaş, C. Falcon, A. Tucholka, J. D. Gispert, J. L. Molinuevo, and G. Deco. A whole-brain computational modeling approach to explain the alterations in resting-state functional connectivity during progression of alzheimer’s disease. *NeuroImage: Clinical*, 16:343–354, 2017.

K. N. Dillen, H. I. Jacobs, J. Kukolja, N. Richter, B. von Reutern, Ö. A. Onur, K.-J. Langen, and G. R. Fink. Functional disintegration of the default mode network in prodromal alzheimer’s disease. *Journal of Alzheimer’s disease*, 59(1):169–187, 2017.

Y. Du, Z. Fu, and V. D. Calhoun. Classification and prediction of brain disorders using functional connectivity: promising but challenging. *Frontiers in neuroscience*, 12:525, 2018.

V. M. Eguiluz, D. R. Chialvo, G. A. Cecchi, M. Baliki, and A. V. Apkarian. Scale-free brain functional networks. *Physical review letters*, 94(1):018102, 2005.

M. Filippi, E. G. Spinelli, C. Cividini, and F. Agosta. Resting state dynamic functional connectivity in neurodegenerative conditions: a review of magnetic resonance imaging findings. *Frontiers in neuroscience*, 13:657, 2019.

A. Fornito, A. Zalesky, and E. Bullmore. *Fundamentals of brain network analysis*. Academic Press, 2016.

J. D. Gibbons and S. Chakraborti. *Nonparametric statistical inference*. CRC press, 2020.

T. M. Gilligan, F. Sibilia, D. Farrell, D. Lyons, S. P. Kennelly, and A. L. Bokde. No relationship between fornix and cingulum degradation and within-network decreases in functional connectivity in prodromal alzheimer's disease. *PloS one*, 14(10):e0222977, 2019.

J. Gonzalez-Castillo and P. A. Bandettini. Task-based dynamic functional connectivity: Recent findings and open questions. *Neuroimage*, 180:526–533, 2018.

M. D. Greicius, G. Srivastava, A. L. Reiss, and V. Menon. Default-mode network activity distinguishes alzheimer's disease from healthy aging: evidence from functional mri. *Proceedings of the National Academy of Sciences*, 101(13):4637–4642, 2004.

X. He, D. S. Bassett, G. Chaitanya, M. R. Sperling, L. Kozlowski, and J. I. Tracy. Disrupted dynamic network reconfiguration of the language system in temporal lobe epilepsy. *Brain*, 141(5):1375–1389, 2018.

Y. He, Z. Chen, and A. Evans. Structural insights into aberrant topological patterns of large-scale cortical networks in alzheimer's disease. *Journal of Neuroscience*, 28(18):4756–4766, 2008.

S. M. Heringa, Y. D. Reijmer, A. Leemans, H. L. Koek, L. J. Kappelle, G. J. Biessels, et al. Multiple microbleeds are related to cerebral network disruptions in patients with early alzheimer's disease. *Journal of Alzheimer's Disease*, 38(1):211–221, 2014.

C. J. Honey, O. Sporns, L. Cammoun, X. Gigandet, J.-P. Thiran, R. Meuli, and P. Hagmann. Predicting human resting-state functional connectivity from structural connectivity. *Proceedings of the National Academy of Sciences*, 106(6):2035–2040, 2009.

W. H. Kruskal and W. A. Wallis. Use of ranks in one-criterion variance analysis. *Journal of the American statistical Association*, 47(260):583–621, 1952.

M. Laakso, H. Soininen, K. Partanen, E. L. Helkala, P. Hartikainen, P. Vainio, M. Hallikainen, T. Hänninen, and P. Riekkinen Sr. Volumes of hippocampus, amygdala and frontal lobes in the mri-based diagnosis of early alzheimer's disease: correlation with memory functions. *Journal of neural transmission-Parkinson's disease and dementia section*, 9:73–86, 1995.

B. Lei, W. Hou, W. Zou, X. Li, C. Zhang, and T. Wang. Longitudinal score prediction for alzheimer's disease based on ensemble correntropy and spatial-temporal constraint. *Brain imaging and behavior*, 13(1):126–137, 2019.

N. Leonardi and D. Van De Ville. On spurious and real fluctuations of dynamic functional connectivity during rest. *Neuroimage*, 104:430–436, 2015.

Z. Liu, Y. Zhang, H. Yan, L. Bai, R. Dai, W. Wei, C. Zhong, T. Xue, H. Wang, Y. Feng, et al. Altered topological patterns of brain networks in mild cognitive impairment and alzheimer's disease: a resting-state fmri study. *Psychiatry Research: Neuroimaging*, 202(2):118–125, 2012.

C.-Y. Lo, P.-N. Wang, K.-H. Chou, J. Wang, Y. He, and C.-P. Lin. Diffusion tensor tractography reveals abnormal topological organization in structural cortical networks in alzheimer's disease. *Journal of Neuroscience*, 30(50):16876–16885, 2010.

L. Lorenzini, S. Ingala, L. E. Collij, V. Wottschel, S. Haller, K. Blennow, G. Frisoni, G. Chételat, P. Payoux, P. Lage-Martinez, et al. Eigenvector centrality dynamics are related to alzheimer's disease pathological changes in non-demented individuals. *Brain communications*, 5(3):fcad088, 2023.

X. Luo, T. Qiu, Y. Jia, P. Huang, X. Xu, X. Yu, Z. Shen, Y. Jiaerken, X. Guan, J. Zhou, et al. Intrinsic functional connectivity alterations in cognitively intact elderly apoe ε4 carriers measured by eigenvector centrality mapping are related to cognition and csf biomarkers: a preliminary study. *Brain imaging and behavior*, 11(5):1290–1301, 2017.

M. P. Mattson. Apoptosis in neurodegenerative disorders. *Nature reviews Molecular cell biology*, 1(2):120–130, 2000.

S. Moguilner, A. M. García, Y. S. Perl, E. Tagliazucchi, O. Piguet, F. Kumfor, P. Reyes, D. Matallana, L. Sedeño, and A. Ibáñez. Dynamic brain fluctuations outperform connectivity measures and mirror pathophysiological profiles across dementia subtypes: a multicenter study. *Neuroimage*, 225:117522, 2021.

P. Núñez, J. Poza, C. Gómez, V. Rodríguez-González, A. Hillebrand, P. Tewarie, M. Á. Tola-Arribas, M. Cano, and R. Hornero. Abnormal meta-state activation of dynamic brain networks across the alzheimer spectrum. *NeuroImage*, 232:117898, 2021.

K. Pearson. VII. note on regression and inheritance in the case of two parents. *proceedings of the royal society of London*, 58(347-352):240–242, 1895.

J. Petrella, F. Sheldon, S. Prince, V. Calhoun, and P. Doraiswamy. Default mode network connectivity in stable vs progressive mild cognitive impairment. *Neurology*, 76(6):511–517, 2011.

M. Pievani, W. de Haan, T. Wu, W. W. Seeley, and G. B. Frisoni. Functional network disruption in the degenerative dementias. *The Lancet Neurology*, 10(9):829–843, 2011.

F. C. Quevenco, M. G. Preti, J. M. Van Bergen, J. Hua, M. Wyss, X. Li, S. J. Schreiner, S. C. Steininger, R. Meyer, I. B. Meier, et al. Memory performance-related dynamic brain connectivity indicates pathological burden and genetic risk for alzheimer’s disease. *Alzheimer’s research & therapy*, 9(1):1–11, 2017.

Y. D. Reijmer, A. Leemans, K. Caeyenberghs, S. M. Heringa, H. L. Koek, G. J. Biessels, U. V. C. I. S. Group, et al. Disruption of cerebral networks and cognitive impairment in alzheimer disease. *Neurology*, 80(15):1370–1377, 2013.

N. Rubido, G. Riedel, and V. Vuksanović. Genetic basis of anatomical asymmetry and aberrant dynamic functional networks in alzheimer’s disease. *Brain Communications*, 6(1):fcad320, 2024.

M. S. Sendi, E. Zendehrouh, C. A. Ellis, J. Chen, R. L. Miller, E. C. Mormino, D. H. Salat, and V. Calhoun. The link between static and dynamic brain functional network connectivity and genetic risk of alzheimer’s disease. *bioRxiv*, 2021.

E. H. Seo, D. Y. Lee, J.-M. Lee, J.-S. Park, B. K. Sohn, D. S. Lee, Y. M. Choe, and J. I. Woo. Whole-brain functional networks in cognitively normal, mild cognitive impairment, and alzheimer’s disease. *PloS one*, 8(1):e53922, 2013.

S.-J. Son, J. Kim, and H. Park. Structural and functional connectional fingerprints in mild cognitive impairment and alzheimer’s disease patients. *PloS one*, 12(3):e0173426, 2017.

J. Song. Amygdala activity and amygdala-hippocampus connectivity: metabolic diseases, dementia, and neuropsychiatric issues. *Biomedicine & Pharmacotherapy*, 162:114647, 2023.

O. Sporns. *Networks of the Brain*. MIT press, 2010.

C. Stam, B. Jones, G. Nolte, M. Breakspear, and P. Scheltens. Small-world networks and functional connectivity in alzheimer’s disease. *Cerebral cortex*, 17(1):92–99, 2007.

C. Stam, W. De Haan, A. Daffertshofer, B. Jones, I. Manshanden, A.-M. van Cappellen van Walsum, T. Montez, J. Verbunt, J. De Munck, B. Van Dijk, et al. Graph theoretical analysis of magnetoencephalographic functional connectivity in alzheimer’s disease. *Brain*, 132(1):213–224, 2009.

C. J. Stam. Modern network science of neurological disorders. *Nature Reviews Neuroscience*, 15(10):683–695, 2014.

B. M. Tijms, C. Möller, H. Vrenken, A. M. Wink, W. de Haan, W. M. van der Flier, C. J. Stam, P. Scheltens, and F. Barkhof. Single-subject grey matter graphs in alzheimer’s disease. *PloS one*, 8(3):e58921, 2013.

V. Vuksanović and P. Hövel. Functional connectivity of distant cortical regions: role of remote synchronization and symmetry in interactions. *NeuroImage*, 97:1–8, 2014.

V. Vuksanović, R. T. Staff, T. Ahearn, A. D. Murray, and C. M. Wischik. Cortical thickness and surface area networks in healthy aging, alzheimer’s disease and behavioral variant fronto-temporal dementia. *International journal of neural systems*, 29(06):1850055, 2019.

V. Vuksanović, R. T. Staff, T. Ahearn, A. D. Murray, and C. M. Wischik. Cortical thickness and surface area networks in healthy aging, alzheimer’s disease and behavioral variant fronto-temporal dementia. *International Journal of Neural Systems*, 29(06):1850055, 2019. doi:10.1142/S0129065718500557.

D. Wang, A. Belden, S. B. Hanser, M. R. Geddes, and P. Loui. Resting-state connectivity of auditory and reward systems in alzheimer’s disease and mild cognitive impairment. *Frontiers in human neuroscience*, 14:280, 2020.

M. W. Weiner, D. P. Veitch, P. S. Aisen, L. A. Beckett, N. J. Cairns, R. C. Green, D. Harvey, C. R. Jack Jr, W. Jagust, J. C. Morris, et al. The alzheimer’s disease neuroimaging initiative 3: Continued innovation for clinical trial improvement. *Alzheimer’s & Dementia*, 13(5):561–571, 2017.

A. I. Wiesman, V. M. Mundorf, C. C. Casagrande, S. L. Wolfson, C. M. Johnson, P. E. May, D. L. Murman, and T. W. Wilson. Somatosensory dysfunction is masked by variable cognitive deficits across patients on the alzheimer’s disease spectrum. *EBioMedicine*, 73, 2021.

Z. Yao, Y. Zhang, L. Lin, Y. Zhou, C. Xu, T. Jiang, and A. D. N. Initiative. Abnormal cortical networks in mild cognitive impairment and alzheimer’s disease. *PLoS computational biology*, 6(11):e1001006, 2010.

A. Zalesky and M. Breakspear. Towards a statistical test for functional connectivity dynamics. *Neuroimage*, 114: 466–470, 2015.

L. Zecca, M. B. Youdim, P. Riederer, J. R. Connor, and R. R. Crichton. Iron, brain ageing and neurodegenerative disorders. *Nature Reviews Neuroscience*, 5(11):863–873, 2004.

D. Zhang, Y. Wang, L. Zhou, H. Yuan, D. Shen, A. D. N. Initiative, et al. Multimodal classification of alzheimer's disease and mild cognitive impairment. *Neuroimage*, 55(3):856–867, 2011.

H. Zhang, C. Meng, X. Di, X. Wu, and B. Biswal. Static and dynamic functional connectome reveals reconfiguration profiles of whole-brain network across cognitive states. *Network Neuroscience*, 7(3):1034–1050, 2023.